Appendix K

Update of the Abrahamson (2000) Directivity Model for Strike-Slip Earthquakes

K-1 Introduction

Somerville et. al (1997) derived directivity scale factors based on the within-event residuals of Abrahamson and Silva (1997) model. To facilitate combining the residuals from different earthquakes, the directivity model used a normalized directivity parameter, X, given by the ratio of the length of the rupture toward the site, S, to the total rupture length, L, as shown in Figure K-1.

Somerville et al. (1999) used the following functional form for the directivity effect for the average horizontal component:

$$\ln(Dir\ Factor) = c_1 + c_2\ X \cos(\theta) \qquad \text{(K-1)}$$

A short-coming of the Somerville et al. (1997) model is that is did not include saturation (with X) that was observed in numerical simulations conducted as part of the Bay Bridge hazard studies. Abrahamson (2000) developed an update to the Somerville et al. (1997) model that was set to include saturation effects constrained for M7.5 earthquakes for a spectral period of 3 seconds.

The Abrahamson (2000) model used the following functional form for the base directivity model:

$$\ln(Dir\ Factor) = \begin{cases} C_1(T) + 1.88\,C_2(T)\,X & for X \le 0.4 \\ C_1(T) + 1.88\,C_2(T)\,0.4 & for X > 0.4 \end{cases} \qquad \text{(K-2)}$$

where $C_1(T)$ and $C_2(T)$ are the coefficients from the Somerville et al. (1999) model. In addition, Abrahamson (2000) introduced a magnitude-dependent and a distance-dependent taper to the directivity factor:

$$T_d(R_{rup}) = \begin{cases} 1 & for R_{rup} \le 30\,km \\ 1 - (R_{rup} - 30)/30 & for 30 < R_{rup} < 60\,km \\ 0 & for R_{rup} \ge 60\,km \end{cases} \qquad \text{(K-3)}$$

$$T_m(M) = \begin{cases} 1 & for M \ge 6.5 \\ 1 - (R_{rup} - 30)/30 & for 6.0 < M < 6.5 \\ 0 & for M < 6.0 \end{cases} \qquad \text{(K-4)}$$

While the Abrahamson (2000) model captured saturation effects, it did not work well for magnitudes that were not close to M7.5 or for periods not close to 3 seconds.

Recently, as part of the NGA project, a new directivity model was developed by Spudich and Chiou (2008) based on the residuals from Next Generation Attenuation Ground

Motion Prediction Equations (NGA GMPEs). As part of the NGA project, this model was reviewed by the NGA developers in terms of its applicability to the NGA GMPEs. The Spudich and Chiou (2008) directivity model is more general in that it includes a radiation pattern term. An issue with this model is that it is not centered on zero for average directivity conditions, implying a change in the median ground motion for average directivity conditions. The NGA developers were unsure of the cause for this shift and how the models should be applied.

Watson-Lamprey (2007) evaluated the within-event residuals from the NGA GMPEs following the same approach as used by Somerville et al. (1999). She found that the directivity effect was about one-half as strong as in the Somerville et al. (1999) model. This was not consistent with the strong directivity effects given in the Spudich and Chiou (2008) model.

As a result, the NGA developers did not make a recommendation with regard to the applicability of the new directivity model to the NGA GMPEs. Rather, a follow-on project to further evaluate the directivity effect was recommended. This follow-on project began in 2010 and is scheduled to be completed in 2012. As part of this follow-on project, Abrahamson and Watson-Lamprey developed an update of the Abrahamson (2000) model based on numerical simulations conducted as part of the NGA project. This updated model is described in this appendix.

K-2. Numerical Simulations Conducted for the NGA Project

To support the NGA ground motion model developers, a large set of 1-D finite-fault kinematic simulations were run for magnitudes 6.5 to 8.2 for strike-slip earthquakes. The simulations were conducted by three modeling groups: URS, UNR, and Pacific Engineering and Analysis. Descriptions of the simulation methods used by these three groups are given in Somerville et al. (2005). The URS and UNR simulations for are the fault normal and fault parallel components and the PEA simulations are for the average horizontal component. In developing the directivity model, only the URS simulations are used.

K-2.1 Simulation Cases

The simulation cases are listed in Table K-1. The ground motions were computed for a minimum of 20 realizations of the source for each scenario. One realization of the source includes a slip distribution – hypocenter combination. For two ruptures (SC and SD), the minimum number of realizations was increased to 30 because the slip models for these two scenarios includes both deep and shallow ruptures to allow an evaluation of the effect of asperity depth. Shallow rupture is defined as having the center of at least one asperity at a depth of 5 km or less.

The hypocenters were constrained to be located in the upper half (positive Y values in Figures 1 and 2) of the rupture with no less than 6 distinct hypocenter locations. The depth distribution of the hypocenters includes both shallow and deep events.

The station locations for the strike-slip are shown in Figures K-2. The stations are located on just one side of the rupture due to symmetry for a vertical strike-slip fault.

K-3 Residuals from Simulations

The finite-fault simulations lead to a large data set of simulated ground motions. For the evaluation of directivity effects, a regression analysis using a simplified model is conducted and the within-event residuals computed.

The directivity scaling from the residuals for T=3 sec for the M7.5 strike-slip scenario (SE) is shown in Figure K-3. The three simulation models show very different directivity effects: the UNR simulations show no directivity effects, the PEA simulations show some directivity effects, and the URS simulations show large directivity effects. The UNR and PEA simulations include randomness in the source that works well for on average, but tends to break up the directivity. Therefore, only the residuals from the URS model are used for this study.

The T=2 second residuals from the URS model are shown in Figures K-4a-d for magnitudes 6.5, 7.0, 7.5, and 7.8, respectively. These plots show that the directivity factor saturates at about 10 km for all four magnitudes. Similar plots of the T=5 seconds residuals are shown in Figures K-5a-d. For the longer period, the directivity factor saturates at about 40 km for all four magnitudes.

K-4 Directivity Model

The within-event residuals, were to the following functional form using ordinary least-squares:

$$\ln(DirFac) = \left[b_2(T)\, s\cos(\theta) - b_1(T)\right] T_1(R_{rup})\, T_2(M) \qquad \text{(K-5)}$$

where M is the moment magnitude, R_{Rup} is the rupture distance, s and θ are the length and angle for segments of the rupture between the site and the hypocenter as described below.

The s and θ terms are computed from the geometry of the site, rupture, and hypocenter. First, the closest point on the rupture to the site is found. The surface projection of this point is called P_1. Next, move along the rupture segments toward the epicenter until either the length of the rupture reaches the saturation distance, s_0, or the epicenter is reached. This point is called P_2.

The s term is the length of rupture between points P_1 and P_2 measured along strike, not just the distance between P_1 and P_2; and θ is the angle between the line P_2-Site and P_1-P_2 (see Figures K-5 and K-6). The saturation distance, s_0, is given by

$$s_0 = MIN\left(c_1, 10 + 20\left(M - 6.0\right)\right) \qquad \text{(K-6)}$$

Distance and magnitude tapers are applied to limit the directivity effect. The tapers are given by:

$$T_1(R_{rup}) = \begin{cases} 1 & for R_{rup} \le 10km \\ (R_{rup} - 10)/30 & for 10km < R_{rup} < 40km \\ 0 & for R_{rup} \ge 40km \end{cases} \quad \text{(K-7)}$$

$$T_2(M) = \begin{cases} 1 & for M \ge 6.5 \\ 2(M-6) & for 6.0 < M < 6.5 \\ 0 & for M \le 6.0 \end{cases} \quad \text{(K-8)}$$

This model provides a good fit to the directivity effect seen in the URS residuals, but it has the same issue as seen in the Spudich and Chiou (2008) model: the mean of the model is not zero over uniformly distributed stations. If this model is applied to the NGA models, then in addition to capturing the directivity effects, there is a shift in the average ground motion.

The goal of this study is to develop directivity factors that can be applied to the NGA GMPEs without changing the median ground motion for average directivity conditions. To meet this goal, the directivity model derived from the simulation residuals was adjusted to remove the mean value for randomly located sites. The directivity model was applied to a uniform grid of sites within 40 km of the rupture, spaced 1 km apart and the mean of the model predictions was computed. The mean was then fit to the following functional form:

$$Mean = \left[\exp\left(a_1 + a_2(8.5 - M)^2\right) + b_1\right] T_1(R_{rup}) T_2(M) \quad \text{(K-9)}$$

The resulting directivity model, centered on zero, has the following form:

$$\ln(DirFac) = \left[b_2\, s\cos(\theta) - \exp\left(a_1 + a_2(8.5 - M)^2\right)\right] T_1(R_{rup}) T_2(M) \quad \text{(K-10)}$$

The coefficients of the model are listed in Table K-2.

The directivity model, given by equation K-10 is compared to the Somerville et al. (1999) and Abrahamson (2000) directivity models in for M6.5 earthquakes Figures K-7a-c for spectral periods of 1, 3, and 5 seconds, respectively. Similar plots are shown in Figures K-8a-c for M7.5 earthquakes for spectral periods of 1, 3, and 5 seconds, respectively. These figures show that the main difference between the new model and the Abrahamson (2000) model is that the saturation distance in the new model varies as a function of period.

The period dependence of the directivity models is compared in Figure K-9. This figure shows that the new model has a peak in the directivity effect as different periods depending on the magnitude. For the larger magnitude earthquakes the peak in the directivity factor is at longer periods than for moderate magnitudes.

REFERENCES

Abrahamson, N. A. (2000). Effects of rupture directivity on probabilistic seismic hazard analysis, Proc Microzonation Conference, Palm Springs.

Hanks, T. C. and W. H. Bakun (2002). A bilinear source-scaling model for M0log A observations of continental earthquakes, Bull. Seism. Soc. Am., 92, 1841-1846.

Spudich, P., and N. Chiou (2008). Directivity in NGA ground motions: Analysis using isochrone theory, *Earthq. Spectra* **24**, no. 1, 299-318.

Somerville, P. G., N. F. Smith, R. W. Graves. and N. A. Abrahamson (1997). Modification of empirical strong ground motion attenuation relations to include the amplitude and duration effects of rupture directivity, Seism. Res. Let, Vol. 68, 199-222.

Watson-Lamprey, J. (2007). In search of directivity, Seism. Soc. Am. Annual Meeting, (Abstract)

Wells, D. and K. Coppersmith (1994). Updated empirical relationships among magnitude, rupture length, rupture area, and surface displacement, Bull Seism. Soc. Am., Vol. 84, 974-1002.

Table K-1. Sources for Strike-Slip Simulations

Event Name	Mag	Area (km^2)	W (km)	L (km)	Dip	Top of Rupture (km)
SA	6.5	325	13	25	90	0
SB	6.5	480	15	32	90	0
SC	6.5	210	10	21	90	0
SD	7.0	1005	15	67	90	0
SE	7.5	3150	15	210	90	0
SF	7.5	4800	15	320	90	0
SG	7.5	2100	15	140	90	0
SH	7.8	6300	15	420	90	0
SI	7.8	3525	15	235	90	0
SJ	8.2	7050	15	470	90	0

Table K-2. Directivity Model Coefficients for Strike-Slip Earthquakes

Period (sec)	c_1 (km)	b_2 (1/km)	a_1	a_2
1	10	0.018	-2.07	-0.061
2	20	0.041	-0.27	-0.201
3	30	0.044	0.32	-0.303
4	40	0.037	0.43	-0.371
5	50	0.034	0.42	-0.391
7	50	0.028	0.22	-0.380
10	50	0.023	0.04	-0.392

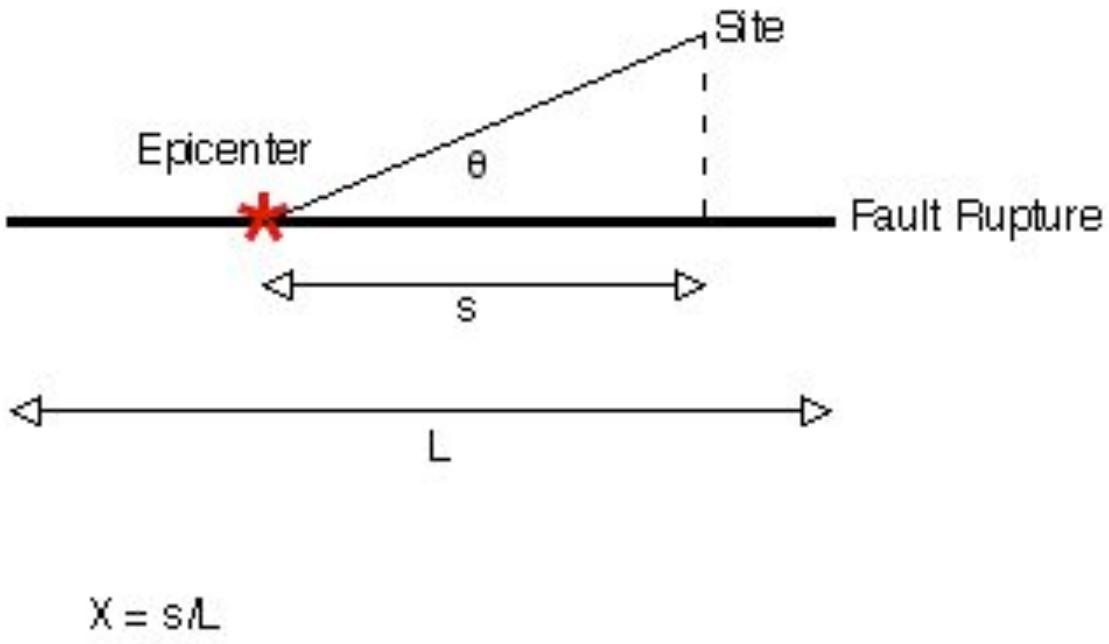

Figure K-1. Directivity parameters for strike-slip earthquakes used by the Somerville et al. (1999).

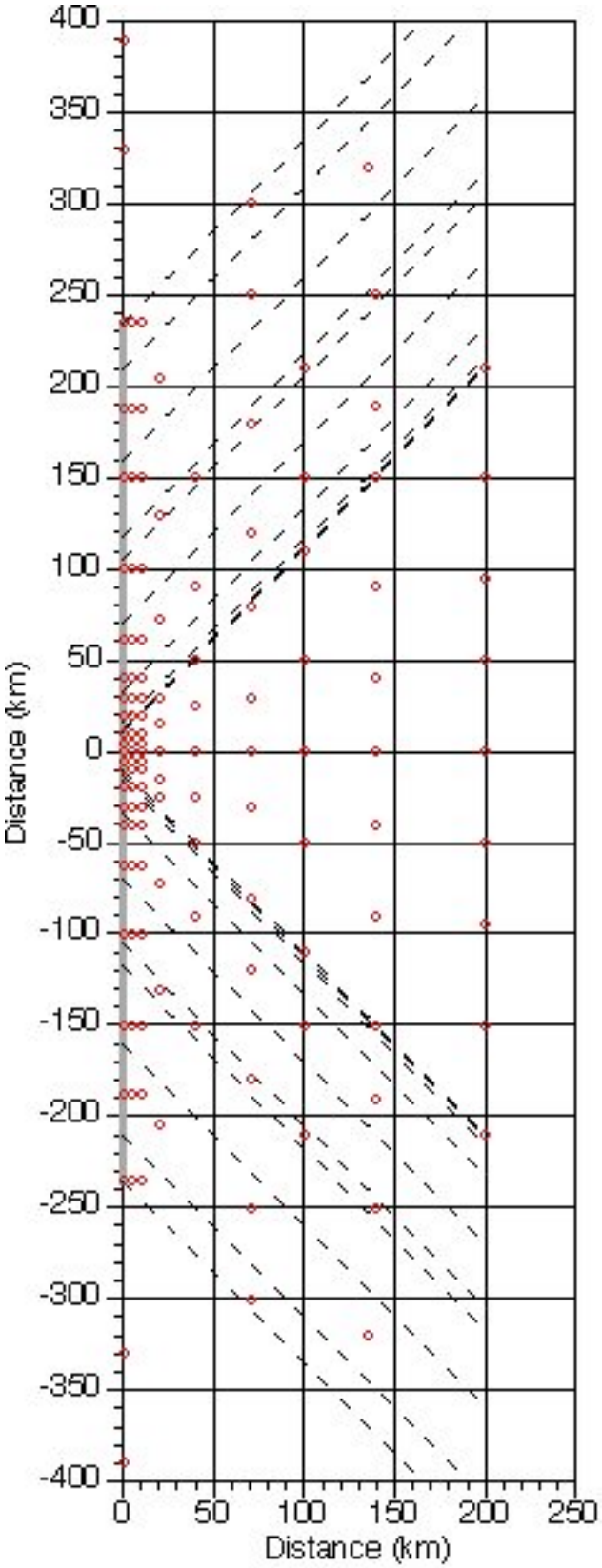

Figure K-2. Station locations for strike-slip simulations.

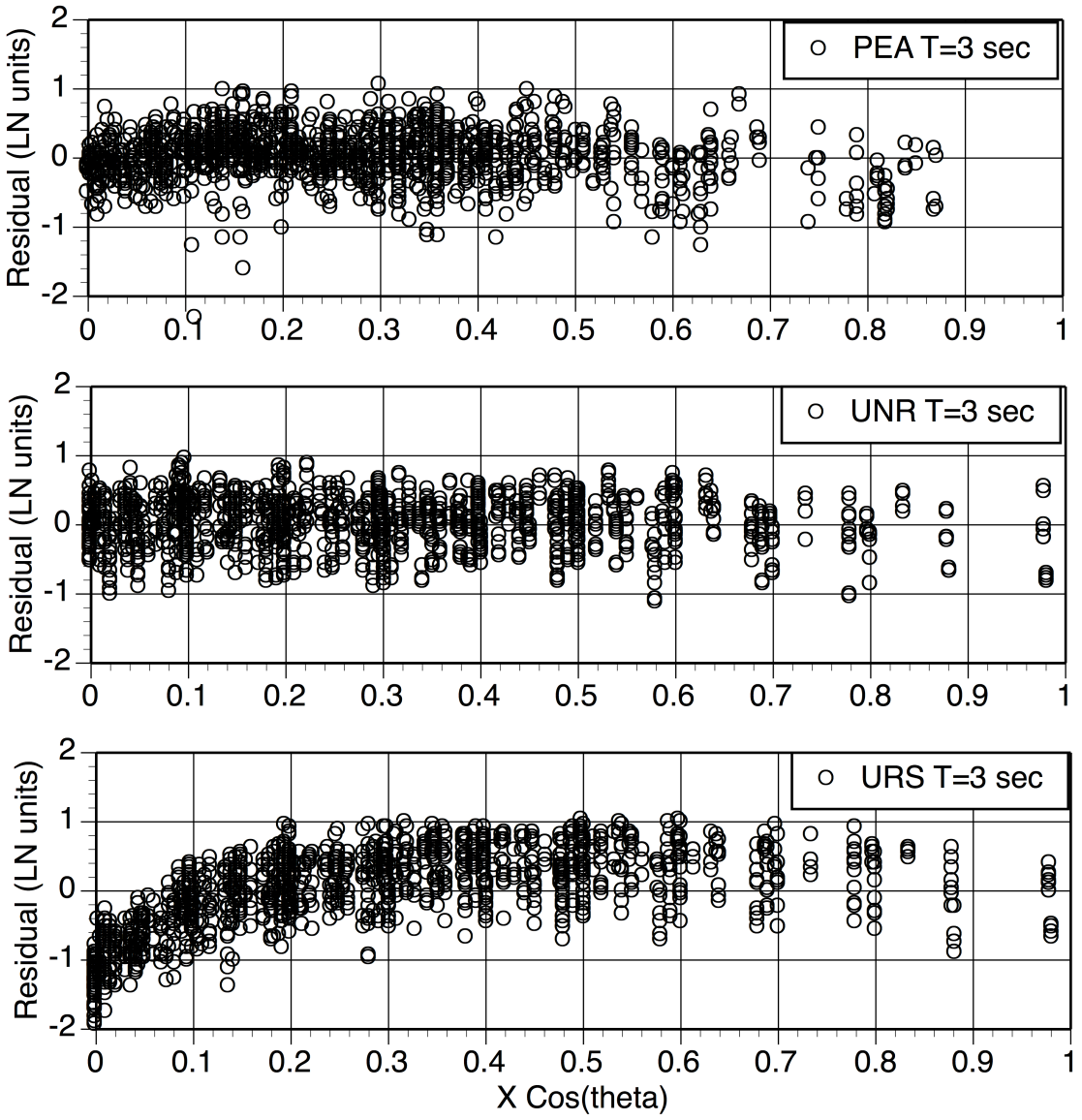

Figure K-3. Comparison of directivity scaling for M7.5 strike-slip (Scenario SE) for T=3 sec for the three different simulation methods.

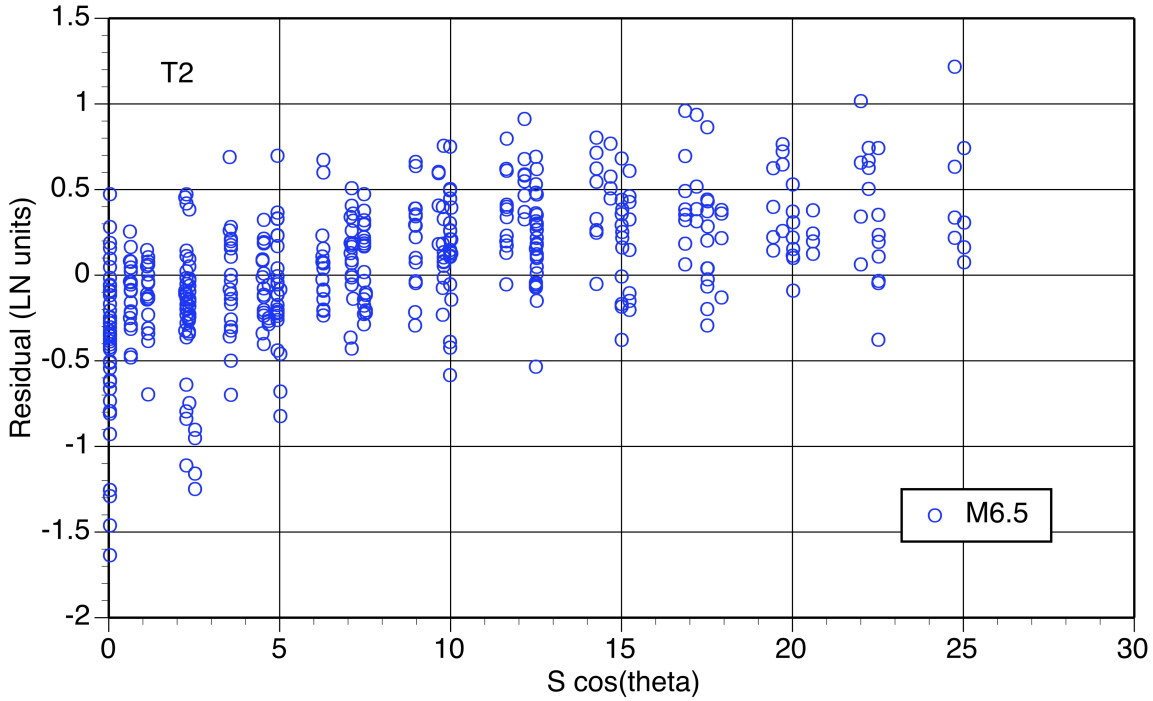

Figure K-4a. Residuals for period T=2 sec and M6.5.

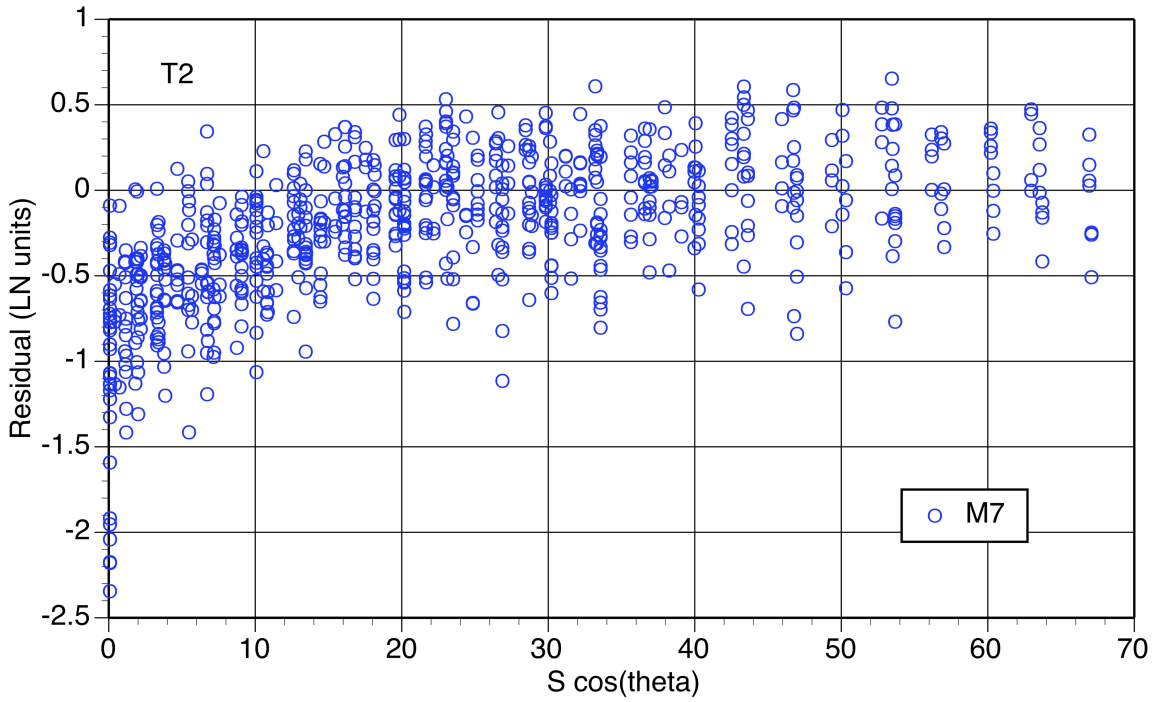

Figure K-4b. Residuals for period T=2 sec, and M7.0.

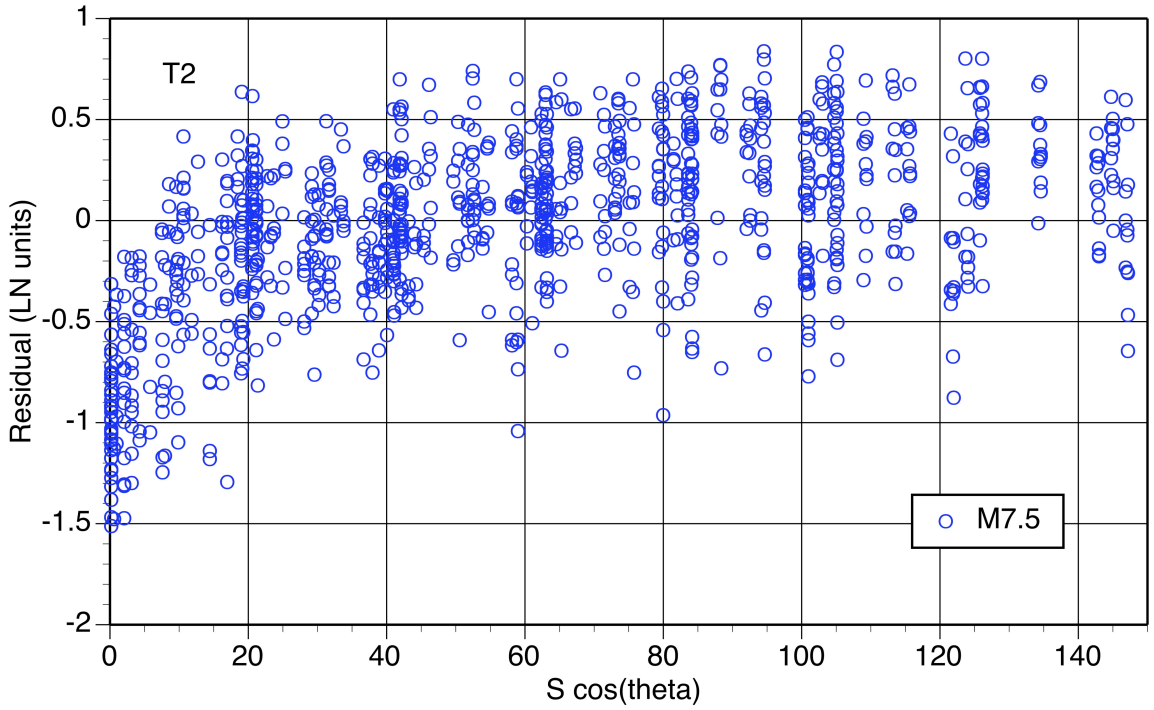

Figure K-4c. Residuals for period T=2 second and M7.5.

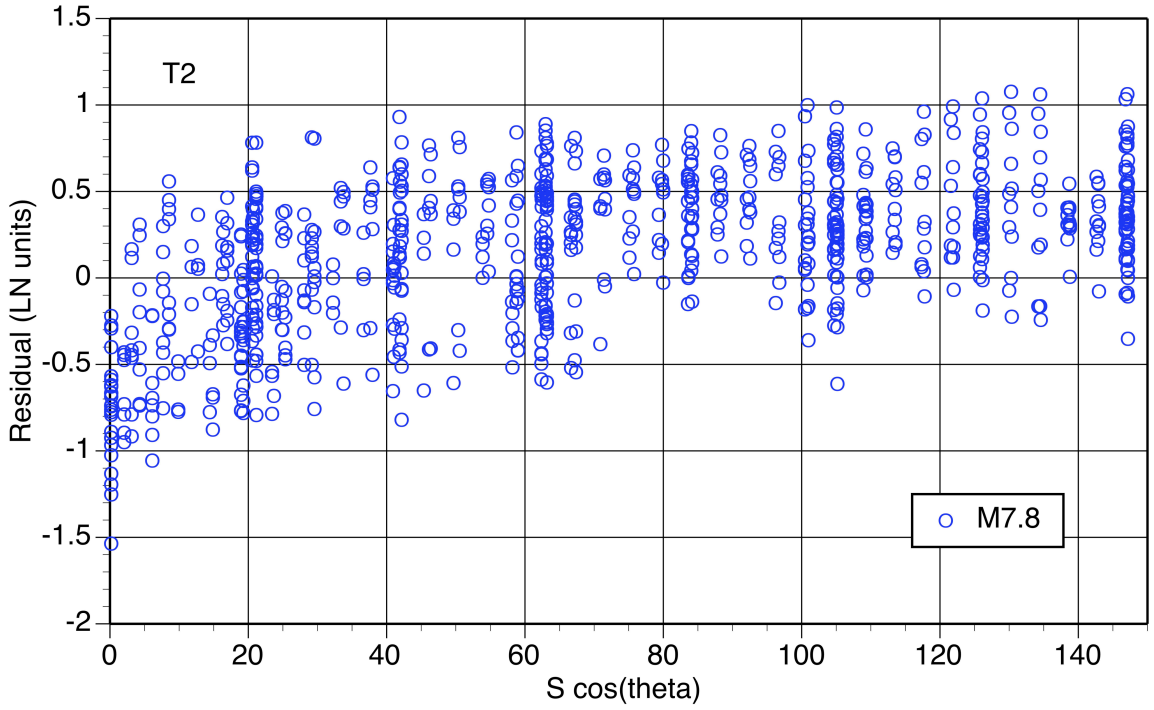

Figure K-4d. Residuals for period T=2 seconds and M7.8.

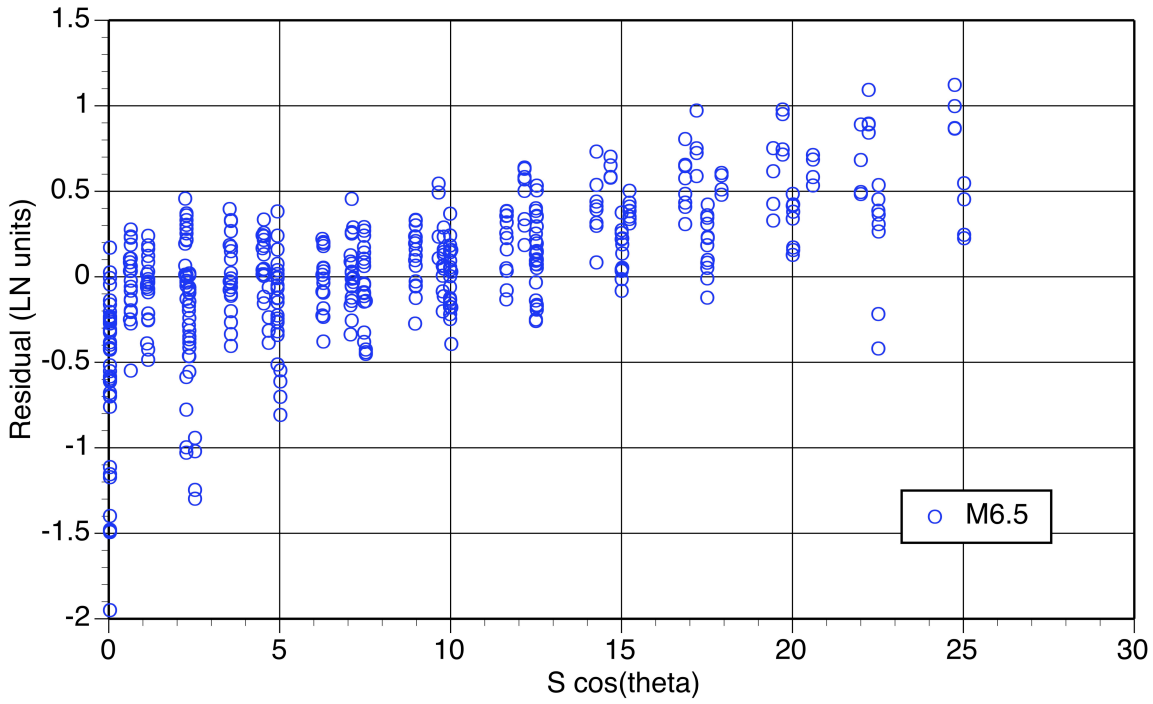

Figure K-5a. Residuals for period T=5 seconds and M6.5.

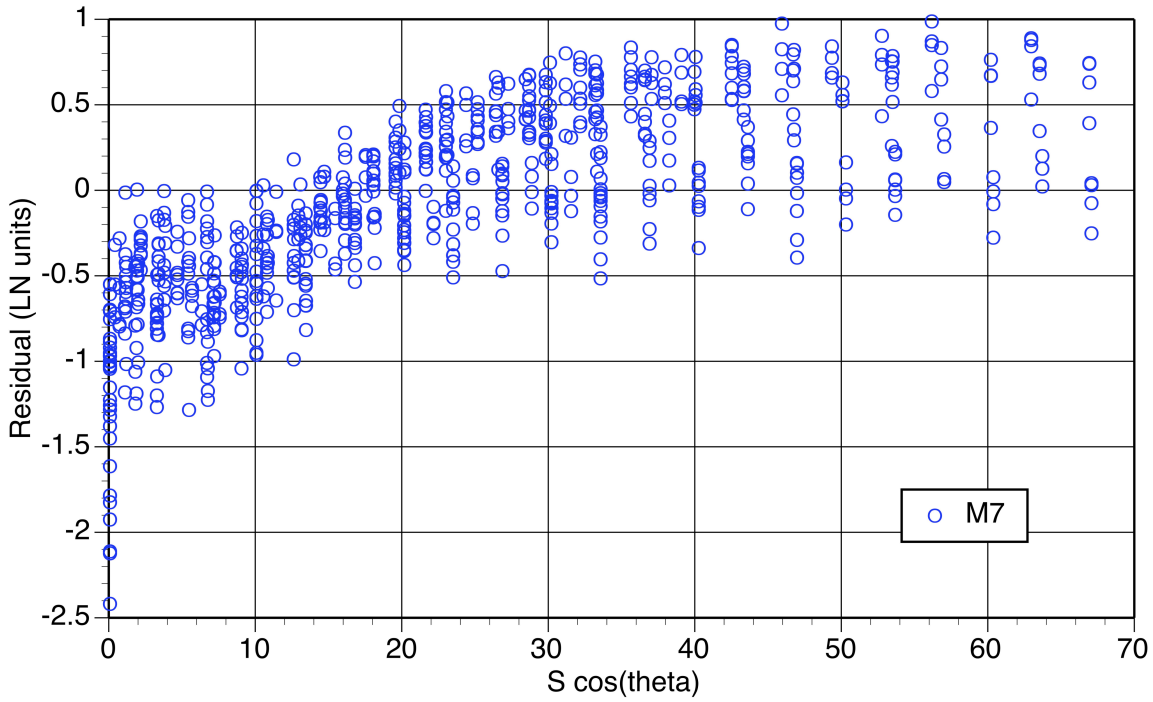

Figure K-5b. Residuals for period T=5 seconds and M7.0.

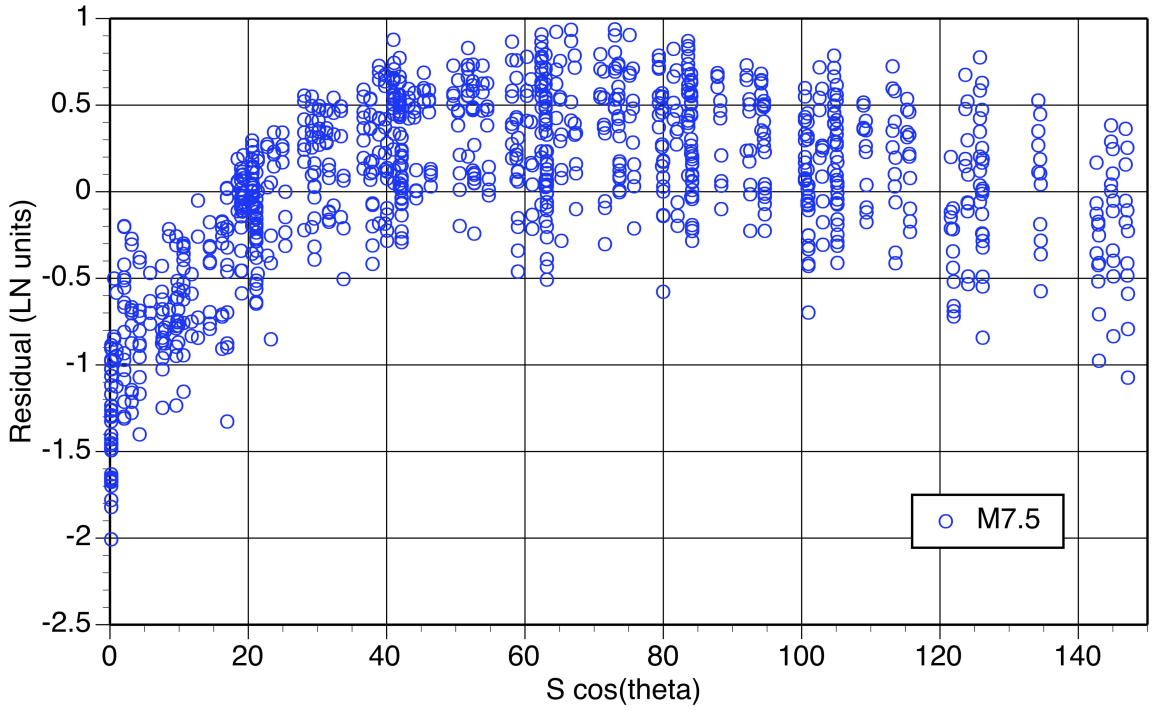

Figure K-5c. Residuals for period T=5 seconds and M7.5.

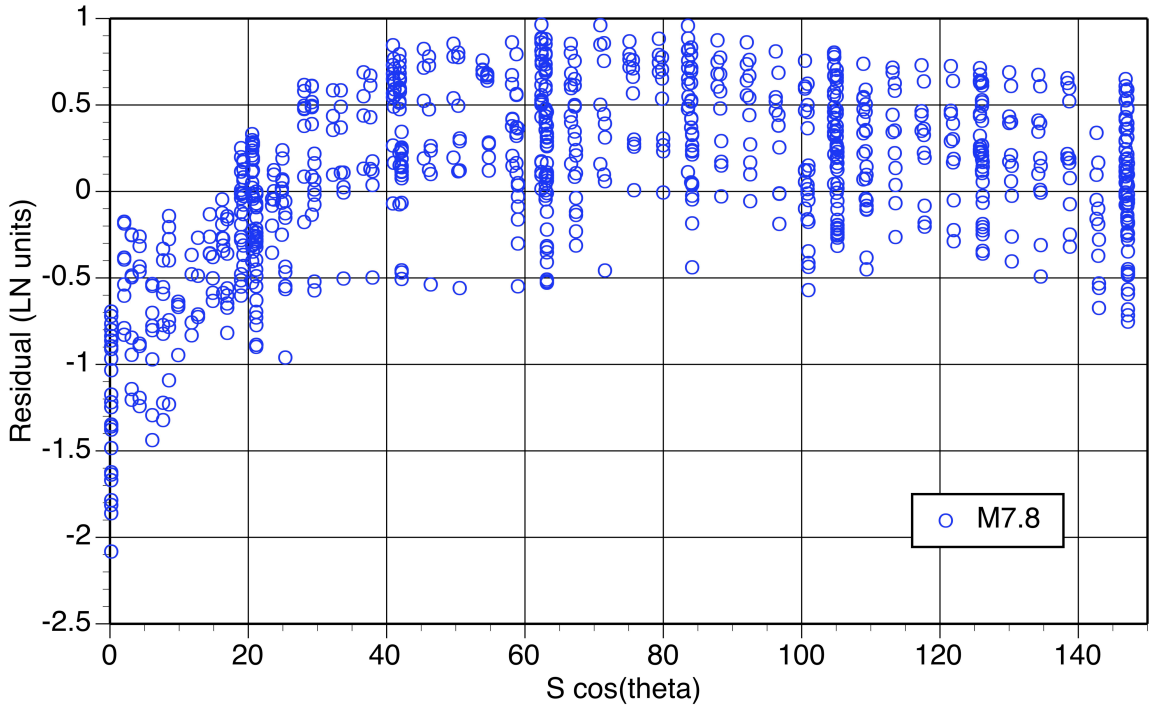

Figure K-5d. Residuals for period T=5 seconds and M7.8.

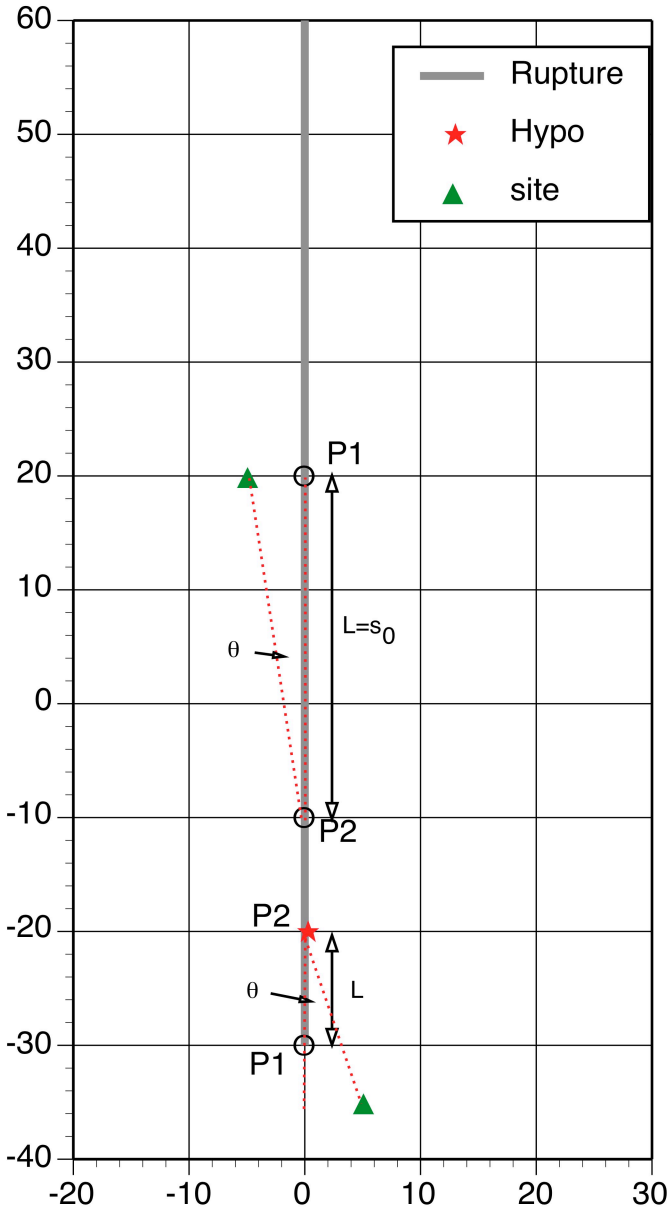

Figure K-6. Examples of the definitions of the segment length and angle for a straight vertically dipping fault. Here, s_0 = 30 km.

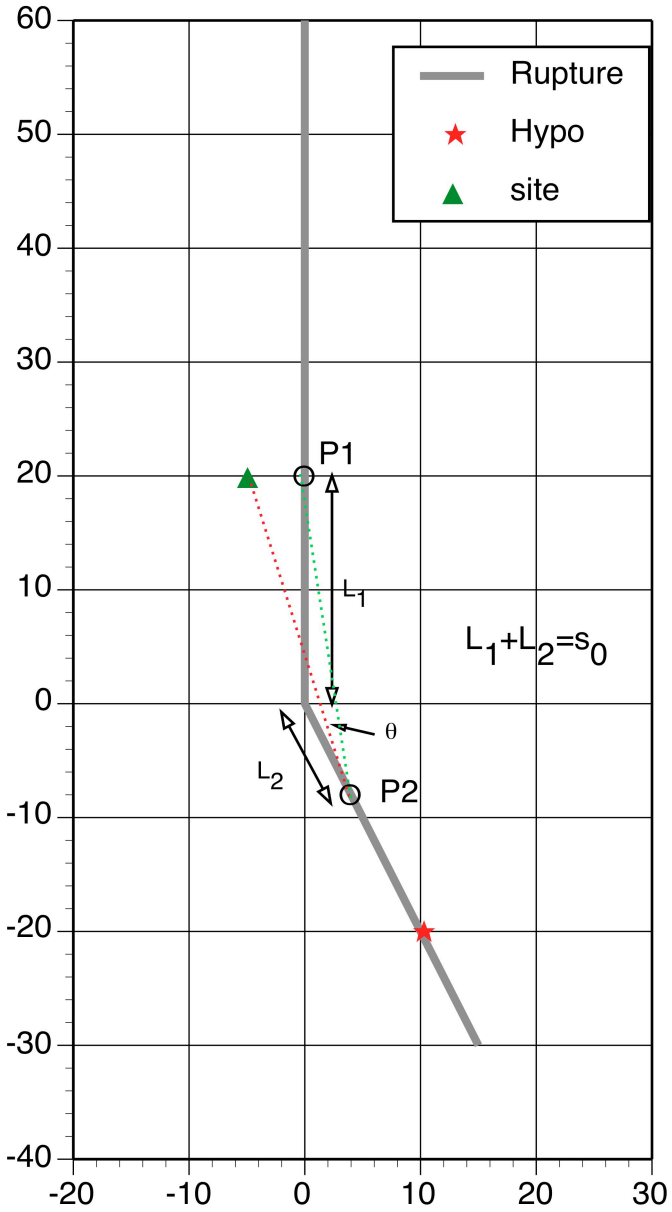

Figure K-7. Example of the definitions of the segment lengths and angle for a bending vertically dipping fault. Here, s_0 = 30 km.

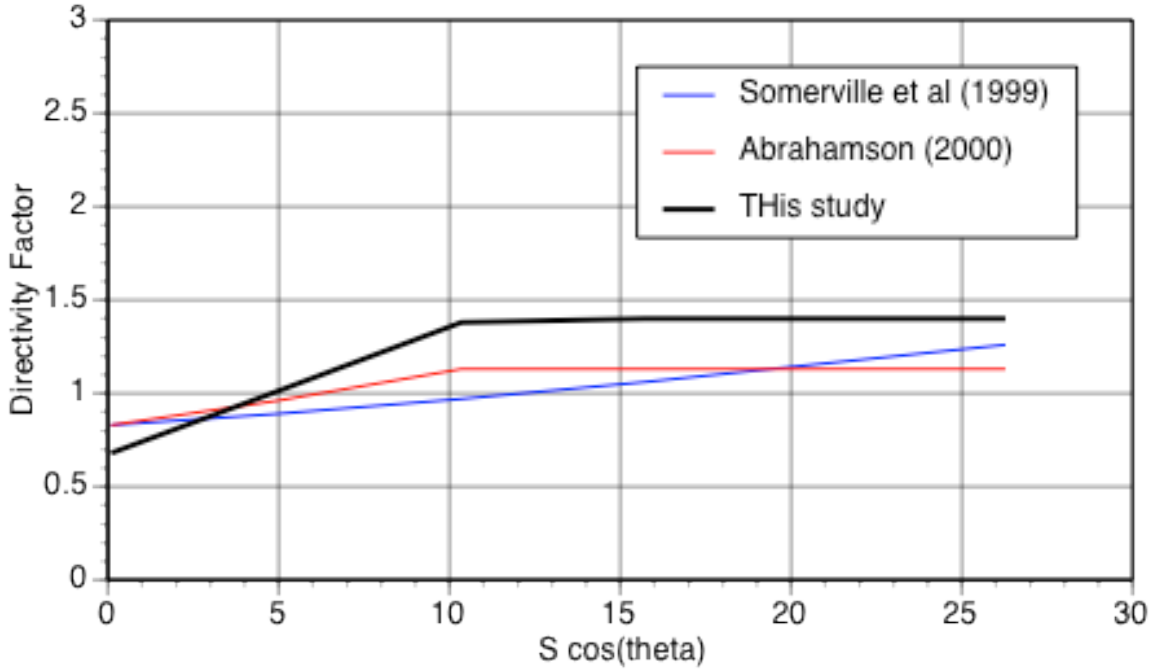

Figure K-8a. Comparison of directivity models for T=1 second period and M6.5.

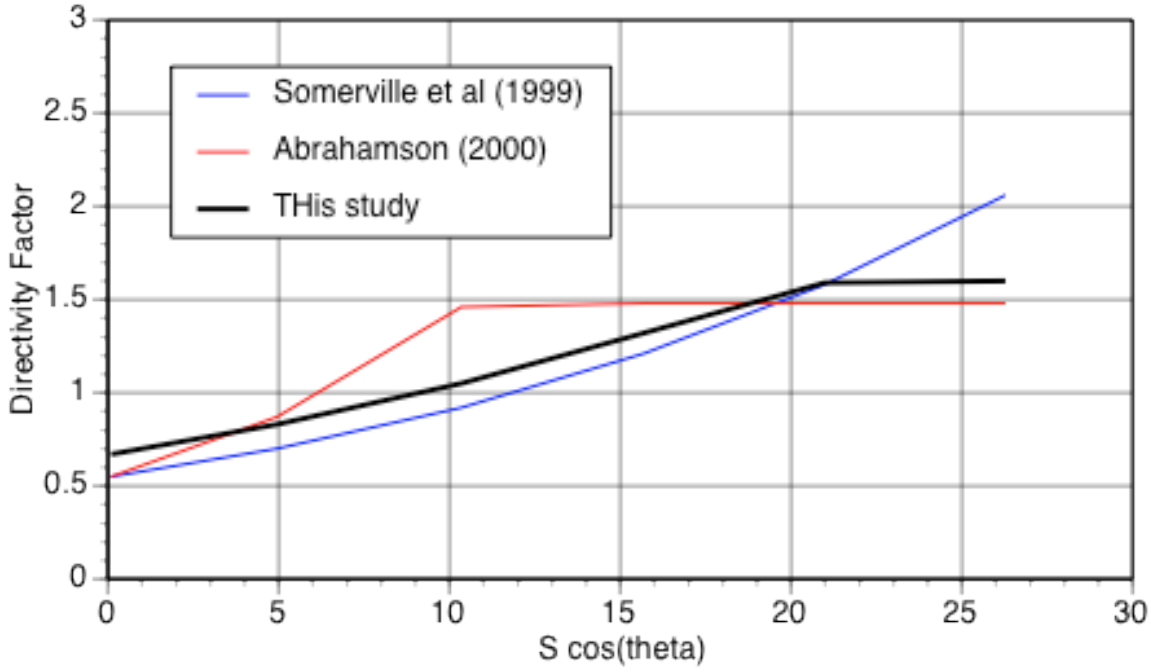

Figure K-8b. Comparison of directivity models for T=3 seconds period and M6.5.

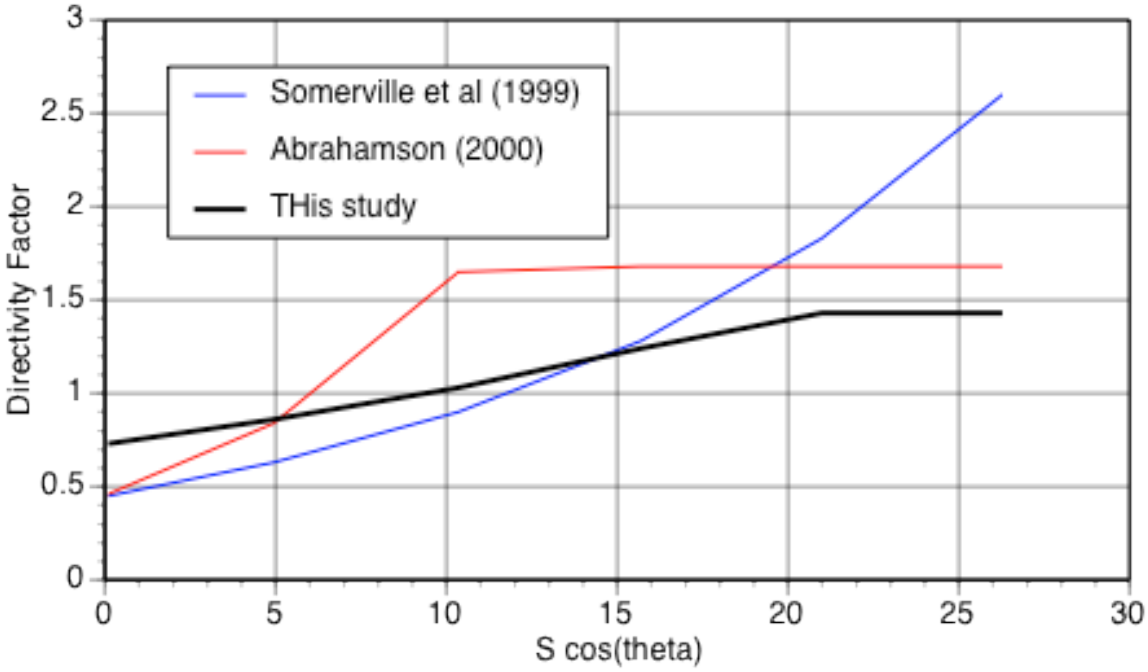

Figure K-8c. Comparison of directivity models for T=5 seconds period and M6.5.

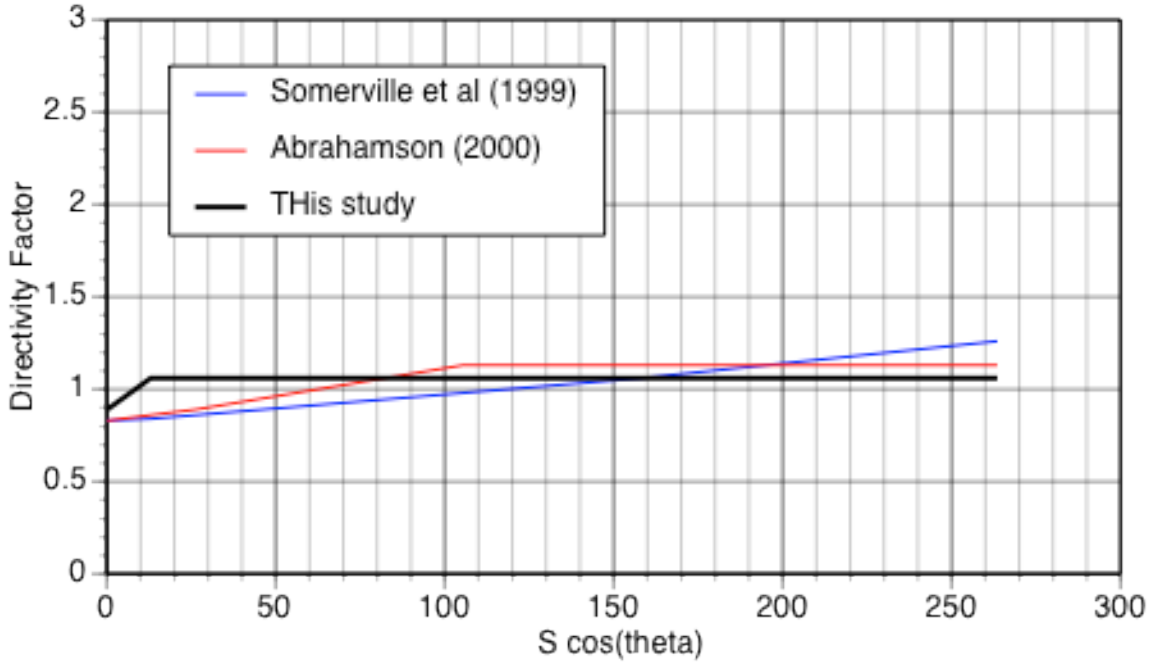

Figure K-9a. Comparison of directivity models for T=1 second period and M7.5.

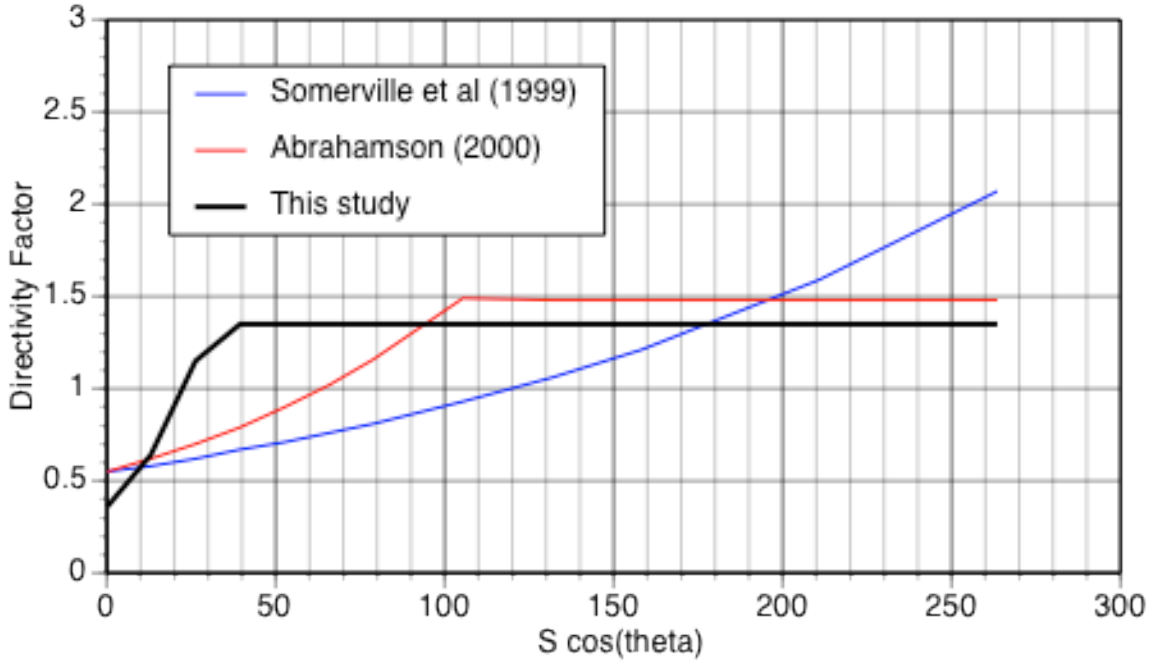

Figure K-9b. Comparison of directivity models for T=3 seconds period and M7.5.

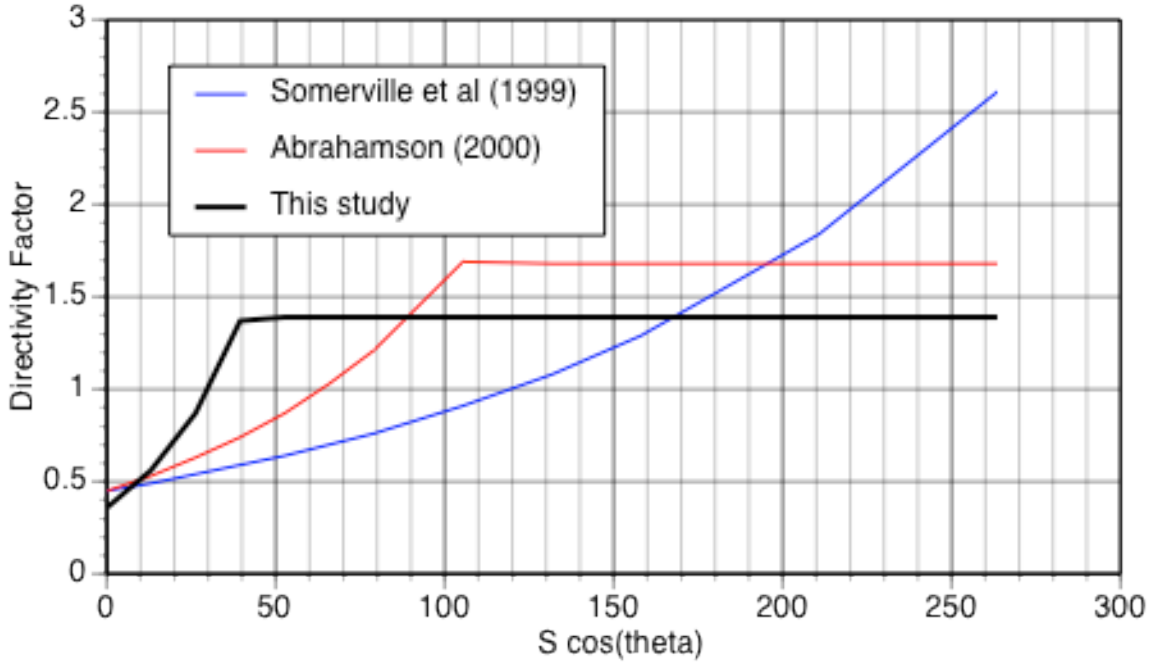

Figure K-9c. Comparison of directivity models for T=5 seconds period and M7.5.

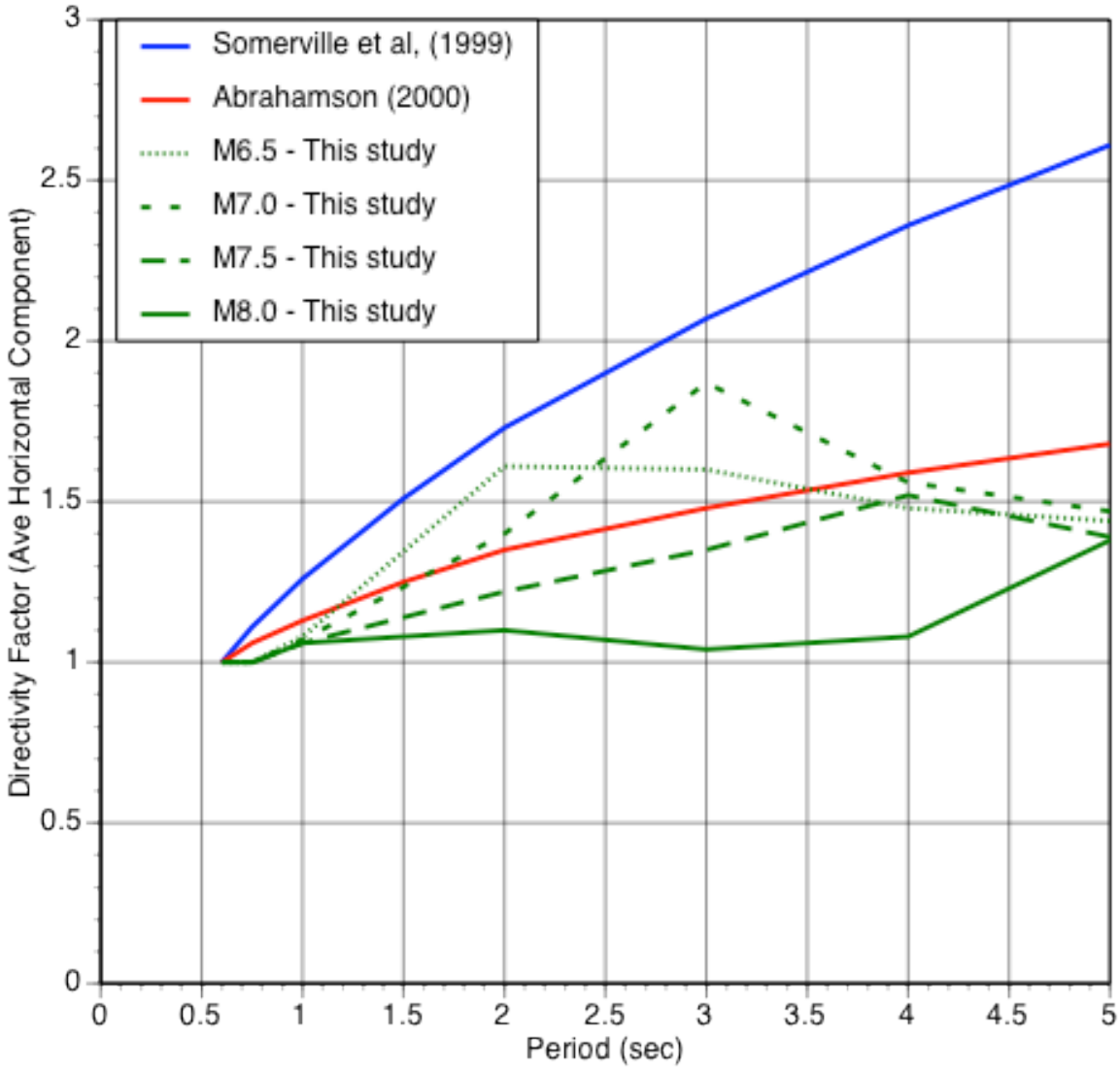

Figure K-8. Comparison of directivity factors for the average horizontal for full directivity (full rupture toward the site) for a site at 1 km distance.